Research Article

Jiliang Xie*, Li Chen, Yanxia Zeng, Xia Sun, and Xin Xiao

# Enhanced electrical conductivity and electromagnetic shielding properties of multi-component polymer/graphite nanocomposites prepared by solid-state shear milling

https://doi.org/10.1515/nleng-2025-0102
received November 19, 2024; accepted February 21, 2025

**Abstract:** This study investigates a novel multi-component polymer composite method for preparing graphite/polymer composites with excellent electrical conductivity and electromagnetic shielding properties, aiming to address the challenges in achieving a balance between conductivity, mechanical stability, and thermal properties in applications like electronics, automotive, and aerospace. Expanded graphite (EG) was used as a conductive filler, and solid-state shear milling was employed to achieve uniform dispersion of graphite in a polymer matrix consisting of polyvinyl chloride (PVC), chlorinated polyethylene (CPE), and polyurethane elastomer (TPU), improving mechanical and thermal stability. X-ray diffraction, Raman spectroscopy, scanning electron microscopy, transmission electron microscopy, and conductivity tests revealed significant differences in graphite dispersion across substrates. In the EG/PVC-CPE system, graphite sheets are stripped into multiple layers, while in the EG/PVC-TPU system, they form thinner or even single layers, leading to enhanced conductivity and shielding efficiency. The results show that the EG/PVC-CPE and EG/PVC-TPU composites offer improved electrical and mechanical properties, demonstrating the potential of multi-component matrices and solid-state shear milling in developing high-performance composites for conductivity and electromagnetic interference shielding applications.

**Keywords:** multi-component polymer composites, graphene, solid state shear grinding, electromagnetic shielding, electrical conductivity

*** Corresponding author: Jiliang Xie**, Institute of Marine Research Development, Jiangsu Ocean University, Lianyungang, Jiangsu, 222005, China, e-mail: jiliangxie@jou.edu.cn
**Li Chen**, **Yanxia Zeng**, **Xia Sun**, **Xin Xiao:** Institute of Marine Research Development, Jiangsu Ocean University, Lianyungang, Jiangsu, 222005, China

## 1 Introduction

Graphene has recently garnered significant attention due to its exceptional electrical, mechanical, thermal, and chemical properties, making it a focal point in the research of polymer matrix composites [1,2]. Its nanoscale thickness and unique two-dimensional layered structure offer immense potential for applications in electronics, energy storage, and sensors [3,4]. However, the strong van der Waals interactions between graphene sheets lead to poor dispersion in polymer matrices, hindering the full utilization of its outstanding physical properties [5,6]. Addressing this challenge has become a critical focus in the field of polymer composites.

Traditional methods, such as liquid-phase exfoliation and chemical vapor deposition, can produce few-layer graphene. However, these methods are often plagued by issues such as poor dispersion effects, low efficiency, and environmental concerns, which limit their practicality in large-scale production [7,8]. Recently, solid-state shear milling (S3M) has emerged as a promising technique for preparing graphene/polymer composites. This method effectively exfoliates graphite and achieves uniform dispersion under solvent-free and environmentally friendly conditions [9,10]. S3M utilizes a high-shear-force field to exfoliate graphite flakes within a polymer matrix, significantly enhancing the mechanical properties, electrical conductivity, and electromagnetic shielding performance of the composites [11,12].

In this study, S3M technology was employed to regulate the exfoliation and dispersion behavior of expanded graphite (EG) within polymer matrices such as polyvinyl chloride (PVC), chlorinated polyethylene (CPE), and polyurethane elastomer (TPU). The process utilized high-efficiency mixing equipment and a disk-type mechanochemical reactor to produce graphenized EG/polymer composite materials [13,14]. Characterization techniques, including X-ray diffraction (XRD), scanning electron microscopy (SEM), transmission electron microscopy (TEM), and Raman

spectroscopy, were applied to analyze the microstructure and exfoliation behavior of the graphite sheets comprehensively. The primary objective was to maximize the exfoliation and dispersion of EG within the polymer matrix while simultaneously improving the mechanical and electrical properties of the composites.

Despite the advancements offered by S3M technology, achieving complete exfoliation and uniform dispersion with a single polymer matrix, such as PVC, remains challenging. Enhancements in the degree of exfoliation and dispersion can be achieved by incorporating viscosity modifiers or elastomers like CPE and TPU. This approach not only facilitates better dispersion of graphite sheets but also further improves the composite material's electrical conductivity and electromagnetic shielding performance.

# 2 Experimental part

## 2.1 Reagents and instruments

PVC: SG-5, particle size 0.1–0.3 mm, Shaanxi Jintai Chlor-Alkali Chemical Co., Ltd. CPE: HG/T2704-2002 135A, Weifang Xingyuan Plastic Co., Ltd. TPU: Bayer385, Bayer Corporation. EG: KP250, Qingdao Nanshu Ruiying Graphite Co., Ltd [15]. Ethylenediamine bismaleimide complex lanthanum (III) heat stabilizer: homemade. Dioctyl phthalate (DOP): Analytically pure, Chengdu McCaxi Chemical Co., Ltd. Mill type force chemical reactor: MF-400 variable frequency type, Chengdu Pumeiyi Technology Co., Ltd.

## 2.2 Preparation process

The preparation route of the composite material is shown in Figure 1.

Disc crusher stages A, B, C, and D show grinding, sliding, peeling, and dispersion. The disc crusher's ring structure is its primary component for generating strong shear forces. When the EG/PVC-TPE composite powder prepared by S3M is diluted by melting and mixing with PVC-TPE, graphene/PVC-TPE nanocomposites with good graphene dispersion can be prepared in PVC-TPE matrix [16].

### 2.2.1 Preparation of EG

The 2.0 g EG was evenly spread in 1,000 mL beaker, then put into a microwave reactor, and removed by 560 W irradiated expansion for 20 s to obtain EG.

### 2.2.2 Preparation of EG/PVC, EG/PVC/CPE, and EG/PVC/TPU composite powders

PVC and EG were combined at a specified mass ratio, with the addition of a 4% ethylenediamine bismaleimide-lanthanum (III) complex as a heat stabilizer. The mixture was initially blended in a high-speed mixer. Subsequently, it was introduced into a grinding disk-type mechanochemical reactor, where grinding was performed at room temperature. During the grinding process, circulating water was used for cooling, while the pressure was regulated

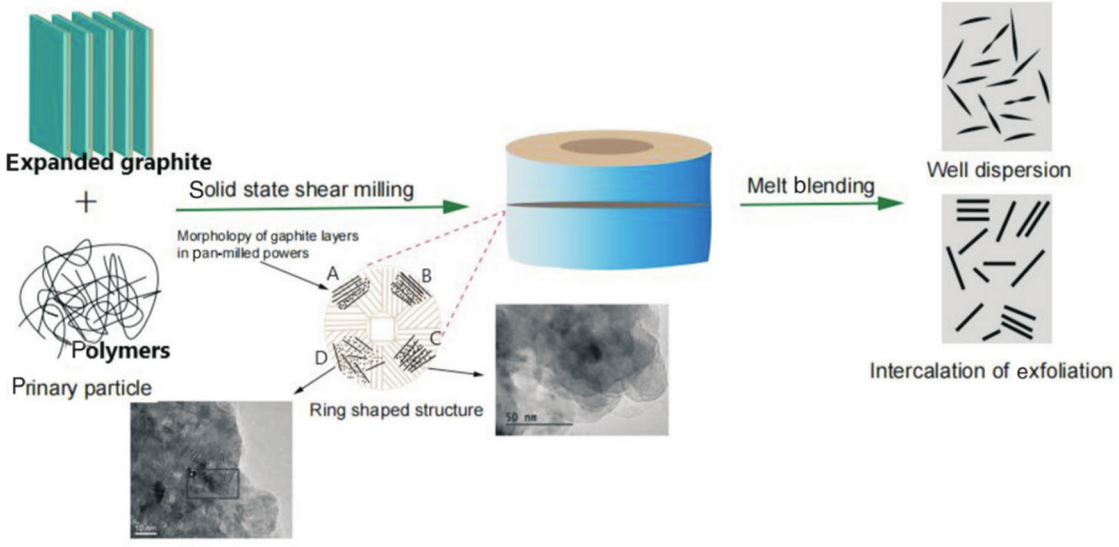


**Figure 1:** Dispersion and spalling of graphite in polymer matrix based on S3M.

using a spiral pressure device. The grinding speed was controlled by an adjustable motor and transmission system [17]. In this experiment, the grinding disk was operated at a speed of 30 rpm, producing EG/PVC composite powder.

Similarly, PVC, CPE, and EG were mixed in a specific ratio, and the resulting blend was processed to obtain EG/PVC-CPE composite powder following the same preparation method used for EG/PVC powder. Additionally, PVC, TPU, and EG were mixed in a defined proportion, and the EG/PVC-TPU composite powder was prepared using the same procedure as that for EG/PVC powder.

#### 2.2.3 Preparation of EG/PVC, EG/PVC-CPE, and EG/PVC-TPU composites

The EG-PVC composite powder was mixed with a certain amount of PVC, 15% DOP and ethylenediamine bismaleimide combined lanthanum (III) complex heat stabilizer in a blender, and the resulting mixed powder was plasticized in a 90°C oven for 3 h. The plasticized powder was directly hot-pressed, and the forming condition was 12.5 MPa, 180°C, 10 min, to obtain EG/PVC composite material. EG/PVC-CPE and EG/PVC-TPU composites were prepared by EG/PVC-CPE and EG/PVC-TPU composite powders using the same process as above.

## 2.3 Examination and description

#### 2.3.1 XRD analysis

The change in graphite layer spacing was determined by X'PERT X-ray diffractometer of Philips Analytical Company with $C_u$ target, $K_\alpha$ radiation source, $N_i$ filter, acceleration voltage of 40 kV, tube current of 25 mA, wavelength of 0.154 nm, and scanning range ($2\theta$) of 0°–50°.

Bragg equation is used to calculate the spacing between crystal faces

$$2d_{hkl}\sin\theta = \lambda. \tag{1}$$

The Scherrer formula is used to calculate lattice parameters or microcrystal sizes

$$D = K\lambda/\beta\cos\theta, \tag{2}$$

where $K = 0.89$; $\lambda = 0.154$ nm; $\beta$ is the diffraction peak's half-peak width (radian) obtained by computer; $\theta$ is the diffraction angle corresponding to the diffraction peak.

#### 2.3.2 SEM analysis

The F-type SEM manufactured by the American FEI Company was utilized to observe the liquid nitrogen-fractured surfaces of composite materials or composite powders after gold sputtering treatment. This technique was used to analyze the morphology of the fractured sections or powders and to capture high-resolution images [18]. The observations were conducted under an acceleration voltage of 10 kV, ensuring optimal imaging quality.

Through SEM imaging, the morphological characteristics of the composite powders and cross-sections were analyzed in detail. The dispersion state of graphite within the polymer matrix was inferred based on the distribution and orientation of graphite sheets observed in the images. This analysis provided critical insights into the effectiveness of the S3M process in achieving uniform dispersion and exfoliation of graphite.

Moreover, SEM characterization enabled the identification of potential agglomeration or clustering of graphite sheets, which could impact the material's electrical and mechanical properties. By correlating the morphological features with other experimental results, such as electrical conductivity and mechanical testing, a comprehensive understanding of the material's structure–property relationship was established. This method is instrumental in optimizing the preparation process to enhance the performance of the composite materials.

#### 2.3.3 TEM analysis

Ultrathin slices of EG/PVC and EG/PVC/CPE composites were made with Leica EMFC6 microslicing machine, and sheets of about 70 nm thick were made, or EG-PVC and EG-PVC CPE composite powders were directly attached to copper mesh, and examined using an H-600 TEM, taking pictures. It has a 75 kV acceleration voltage. The dispersion and peeling state of graphite in the composite system and the nanocomposite structure of the composite were characterized.

#### 2.3.4 Atomic force microscope (AFM) analysis

The analysis was carried out with Innova AFM produced by Veeco, USA. The resolution was <0.2 μm and the standard 10× objective lens was observed (50× objective lens < μm). Sample preparation: The composite powder was dispersed in *N*-methylpyrrolidone (NMP) (0.1 g composite powder/100 mL NMP), and the ultrasonic power was 600 W for 10 min. The composite powder was coated on the silicon wafer for observation and analysis.

#### 2.3.5 Laser Raman analysis

InVia laser Raman spectrometer, with $Ar^+$ laser, wavelength 514.5 nm, scanning range of 1,000–3,000 $cm^{-1}$, and accuracy of ±1 $cm^{-1}$ was used.

#### 2.3.6 Laser particle size analysis

With a beam length of 2.50 mm and a pump speed of 2,400 rpm, the Mastersizer laser particle size analyzer manufactured by Malvern Instruments Co., Ltd was used to investigate the particle size distribution of EG-PVC composite powder.

#### 2.3.7 Conductivity test

At room temperature, the sample resistivity was measured with ZC46A high resistance meter produced by Shanghai Precision Scientific Instrument Co., Ltd. The measuring voltage was 50 V and the measuring range was 106–1,014 Ω. The resistance of the composite material is less than 106 Ω. Use a multimeter to detect the composite material (the sample length × width × thickness is 10 cm × 1 cm × 0.1 cm).

#### 2.3.8 Electromagnetic shielding performance analysis

The PNA-N5244A vector network analyzer from Agilent Technologies was employed to measure the S-scattering parameters of the composite materials, which were subsequently used to calculate the electromagnetic interference (EMI) shielding effectiveness (EMI SE). The testing was conducted using a coaxial approach to ensure precision and reliability in the measurements.

The test frequency range spanned from 2 to 18 GHz, covering a wide spectrum of electromagnetic waves relevant to practical applications. Samples were prepared in the form of coaxial rings with precise dimensions: an outer diameter of 7 mm, an inner diameter of 3 mm, and a thickness of 1 mm. These dimensions were chosen to fit the standard testing setup, ensuring consistency and comparability with other studies.

The coaxial measurement method allowed for accurate evaluation of the shielding performance by minimizing edge effects and ensuring uniform electromagnetic wave propagation through the samples. The obtained S-parameters (S11 and S21) provided detailed insights into the reflection, absorption, and transmission characteristics of the composite materials, enabling a comprehensive analysis of their electromagnetic shielding properties.

Additionally, the results from the vector network analyzer were used to validate the dispersion and exfoliation of graphite in the polymer matrix, as improved dispersion is directly correlated with enhanced electromagnetic shielding efficiency. This approach highlights the composite's potential for applications in electronics, telecommunications, and aerospace, where effective EMI shielding is critical.

#### 2.3.9 Mechanical properties test

Instron5507 universal material testing machine was used to test the tensile properties of the samples according to GB/T 1040, and the tensile speed was 10 mm/min.

# 3 Findings and discussion

## 3.1 Preparation of EG

Figure 2 shows the SEM photo of EG prepared by microwave irradiation expansion. It shows that EG is composed of many bonded and superimposed graphite scales. Under

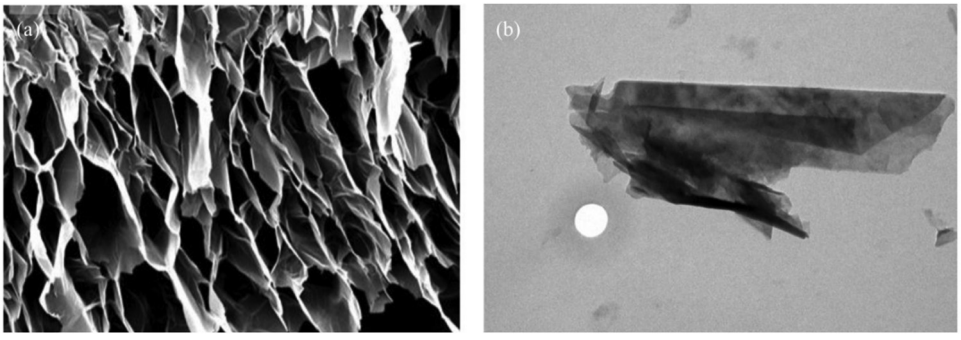


**Figure 2:** SEM images of EG prepared by (a) high-temperature expansion and (b) microwave-irradiation expansion.

**Table 1:** Properties of EG prepared by microwave irradiation

| Expanding process | Expansion volume/(mL $g^{-1}$) | Specific area/($m^2$ $g^{-1}$) | Pore volume/($cm^3$ $g^{-1}$) | Mean pore size/(nm) |
|---|---|---|---|---|
| Microwave irradiation in 560 W for 20 s | 288 | 61.747 | 0.16 | 83.5 |

the action of expansion, the specific surface area of EG increases, there are many honeycomb microvoids between the lamella, the lamellar structure remains, the interlamellar distance increases, and the lamella becomes thinner.

Table 1 shows that EG prepared by microwave irradiation KP250 has the characteristics of high specific surface area, high volume expansion rate, and small pore volume, and average pore size, which proves that microwave irradiation is a better way to prepare EG.

## 3.2 Solid phase shear graphenization of EG

In the solid-phase co-milling of EG-PVC, the lamellar stripping of graphite and the formation of nanocomposites with PVC were achieved using a grinding disk-type mechanochemical reactor, which creates a strong shear force field. However, XRD, TEM, and Raman spectroscopy demonstrated that after 100 milling cycles, the graphite sheets in the EG-PVC system were still above five layers thick, indicating that complete graphenization of the EG was not achieved. This was primarily due to the insufficient viscosity of the polymer matrix [19].

To improve the viscosity of the polymer and facilitate better dispersion of graphite, CPE elastomer was added to the EG-PVC system. XRD, TEM, and Raman analysis of the CPE-EG-PVC system, after 40 milling cycles, revealed that the thickness of the graphite sheets was reduced to 3–4 nm. Considering the measured single-layer graphene thickness of 0.4–0.7 nm, the graphite sheets were approximately five layers thick, indicating that the material had reached a graphene-like structure. To further enhance the dispersion and exfoliation, CPE was substituted with the commercially available Bayer 385 TPU. When TPU-EG-PVC was milled for 40 rounds, the thickness of the graphite sheets was reduced to 1–4 nm, with the graphene sheets being approximately 1–5 layers thick.

Figure 3 shows the XRD patterns of EG-PVC (mass ratio 10/90), CPE-EG-PVC, and TPU-EG-PVC (mass ratio 10/10/80) composite powders after 40 milling cycles, while Table 2 presents the changes in key XRD parameters. From EG-PVC to CPE-EG-PVC to TPU-EG-PVC, the diffraction angle of the graphite phase increases, and the interlayer spacing (d-spacing) decreases. The XRD analysis also shows that the composite system with CPE exhibits the highest diffraction intensity and the largest half-peak width, indicating the most extensive exfoliation and peeling of the graphite sheets. In contrast, the TPU-EG-PVC system exhibits the lowest diffraction intensity, suggesting a further reduction in the thickness of the graphene lamellae.

**Table 2:** XRD parameters of cobalt powder

| Composite system | $2\theta$(°) | *D* (002)/(nm) | Peak height | Peak full width at half maximum |
|---|---|---|---|---|
| EG-PVC | 26.35 | 0.339 | 200 | 0.65 |
| CPE-EG-PVC | 26.44 | 0.338 | 181 | 1.19 |
| TPU-EG-PVC | 26.55 | 0.333 | 125 | 0.66 |

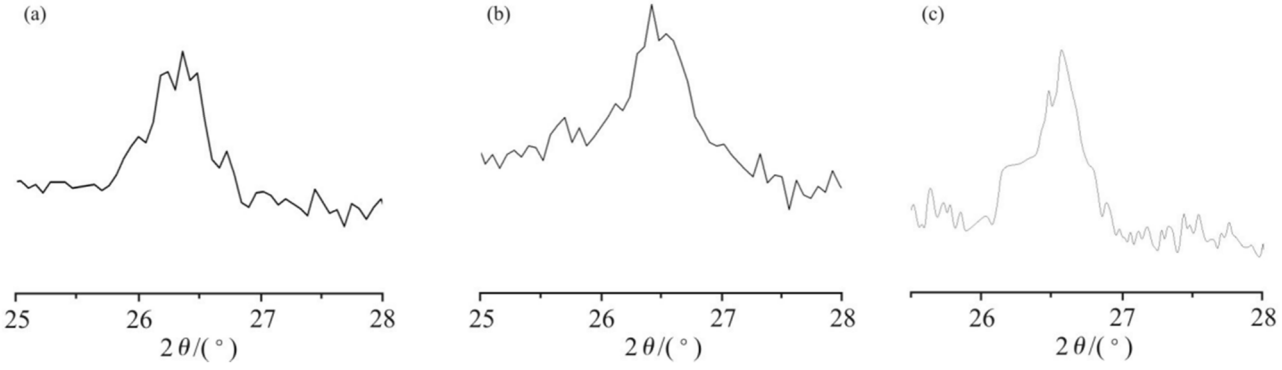


**Figure 3:** XRD patterns of different composite powders. (a) EG-PVC; (b) CPE-EG-PVC; (c) TPU-EG-PVC.

These results demonstrate that the addition of CPE and TPU significantly improves the exfoliation and dispersion of EG in the polymer matrix. The reduction in the stacking thickness of the graphite sheets enhances the material's potential for high electrical conductivity and electromagnetic shielding properties, making the modified composites more suitable for advanced applications.

Figure 4 shows the Raman spectra of $Ar^+$ laser with wavelength of 514.5 nm for scanning EG and EG-PVC, CPE-EG-PVC, TPU-EG-PVC composite powders in the range of 500–3,000 $cm^{-1}$. It is shown that EG has obvious Raman peaks at 1,356 $cm^{-1}$ (D peak), 1,585 $cm^{-1}$ (G peak), and 2,702 $cm^{-1}$ (2D peak). The G peak near 1,585 $cm^{-1}$ in the figure comes from the plane vibration of first-order $E_{2g}$ phonons, reflecting the symmetry and order of the material. The more graphene layers there are, the stronger the $sp^2$ vibration of carbon atoms, the higher the G peak strength, and the stronger the G peak of EG, indicating the relatively orderly structure of EG. The appearance of D peak at 1,356 $cm^{-1}$ indicates that part of the $sp^2$ hybrid carbon atoms in EG are converted into $sp^3$ hybrid structure, that is, the C═C double bond in the graphite layer is destroyed, which is mainly due to the destruction of the graphene structure after oxidation and expansion of graphite, and the graphite oxide cannot be completely reduced during the expansion process. The 2D peak near 2,700 $cm^{-1}$ is a Raman peak for biphonon resonance, the intensity of which indicates the degree of graphene packing, while the ratio of G peak to 2D peak intensity ($I_G/I_{2D}$) is correlated with the quantity of graphene layers. The smaller the $I_G/I_{2D}$ ratio, there are fewer layers of graphene. The graphite sheet is thick, as shown by the figure's comparatively prominent 2D EG peak. The half-peak width of peak G is 24 $cm^{-1}$, and the half-peak width of peak 2D is 136 $cm^{-1}$, indicating that the thickness of the graphite sheet is more than five layers of carbon atoms. The peak strength of the D and G peaks of the EG-PVC composite powder in 1,342 $cm^{-1}$ (D peak), 1,570 $cm^{-1}$ (G peak), and 2,692 $cm^{-1}$ (2D peak) were significantly reduced, indicating that the thickness of the graphite lamellae was reduced, and the regularity of the graphite lamellae was reduced, which proved that the EG layer was slipping and peeling during the grinding process. The peak intensity of peak D and peak G of EG increased, indicating that $sp^3$ hybrid carbon atoms increased, indicating that some $sp^2C$ converted to $sp^3C$, which was mainly attributed to the grinding process, the strong shear force caused C═C double bonds and carbon atoms missing, destroying the mesh structure of graphene, so that some $sp^2C$ converted to $sp^3C$. The 2D peak's half-peak width at 2,692 $cm^{-1}$ decreased to 92 $cm^{-1}$, and was also significantly lower than that at 136 $cm^{-1}$, $I_G/I_{2D}$ = 0.68, $I_G/I_{2D}$ = 6.68, indicating that the graphite lamellae had been stripped and thinned, but the graphene stacking thickness was still more than five layers.

Figure 5 presents the TEM images of the EG-PVC composite powder obtained after 40 milling cycles, with the black areas representing the graphite sheets. Figure 5(a) shows a view perpendicular to the graphene benzene ring structure, where the disordered striped morphology and the intercalation of PVC and graphite are clearly visible. Figure 5(b) displays a local magnification of image (a), offering a closer look at the graphite lamellae. It is evident that the graphite sheets are thinner and interlaced, with a thickness of approximately 10 nm, which aligns with the XRD analysis results. Figure 5(c) illustrates a parallel plane view of the graphene benzene rings, where large thin graphite sheets are stacked on top of each other, indicating that the graphite has undergone partial exfoliation. However, some regions still contain thicker lamellae, likely because not all EG was subjected to the same number of grinding cycles. This uneven milling could be due to variations in the grinding process, where some composite powder may have received less milling due to machine-related factors.

Figure 5(d) presents the TEM image of the composite powder after ultrasonic dispersion in a solvent. In this

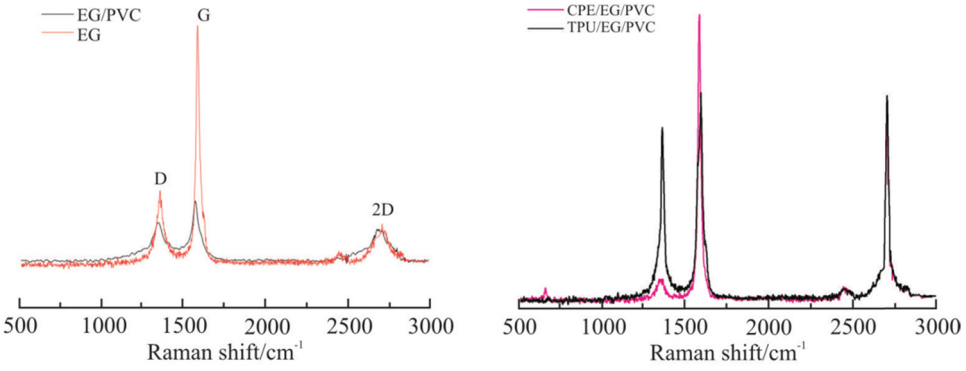


**Figure 4:** Raman spectra of EG and EG-PVC, CPE/EG/PVC, and TPU-EG-PVC.

image, the graphite sheets' large surface area and curled edges are clearly visible, further confirming the exfoliation and dispersion of the graphite in the polymer matrix. The dispersion method enhances the uniformity of the graphite sheets in the composite, contributing to improved properties such as electrical conductivity and mechanical strength.

These TEM observations provide valuable insight into the structural characteristics of the EG-PVC composites, highlighting the effects of grinding and ultrasonic dispersion on the exfoliation and dispersion of graphite within the polymer matrix. The reduced thickness of the graphite sheets and the successful exfoliation are key factors in enhancing the material's performance in various applications.

Figure 6 is the TEM photo of the EG-PVC-CPE composite powder obtained by grinding 40 times, in which the black part is the graphite layer. Figure 6(c) shows the vertical graphene benzene torus field of view, in which the disordered striped structure and the mutual embedding of PVC and graphite can be seen. Figure 6(d) shows the local amplification of (c), which more intuitively shows the graphite lamellar thinning and interlacing with each other. The lamellar thickness is about 1 nm, that is, the thickness of two layers of graphene. In the vertical graphene-benzene torus observed in Figure 6(a), EG has been stripped, as seen by the huge, thin layers of graphene sheets that are visible. The composite powder's TEM image following dissolving by ultrasonic is shown in Figure 6(b). The illustration shows the size of the graphite sheet and the curled edge.

In summary, through EG/PVC co-milling, and then the co-milling of EG/PVC-CPE, the graphene of EG is realized, and the thickness of the sheet is about five layers, reaching the level of graphene-like; Furthermore, EG/PVC-TPU co-milling achieves the graphenization of EG in polymer matrix and the nanocomposite with polymer (as shown in Figure 7). It is evident that TPE is essential for EG's graphenization. Through the weak interlayer contact between the viscoelasticity of the polymer and EG, TPE modifies the viscoelasticity of the polymer and depends on the strong three-dimensional shear force field supplied by the mill-type mechanochemical reactor. In the co-milling of EG-TPE-PVC, the process of interface friction, tensile deformation dislocation, extrusion Mosaic, tensile slip, shear stripping and

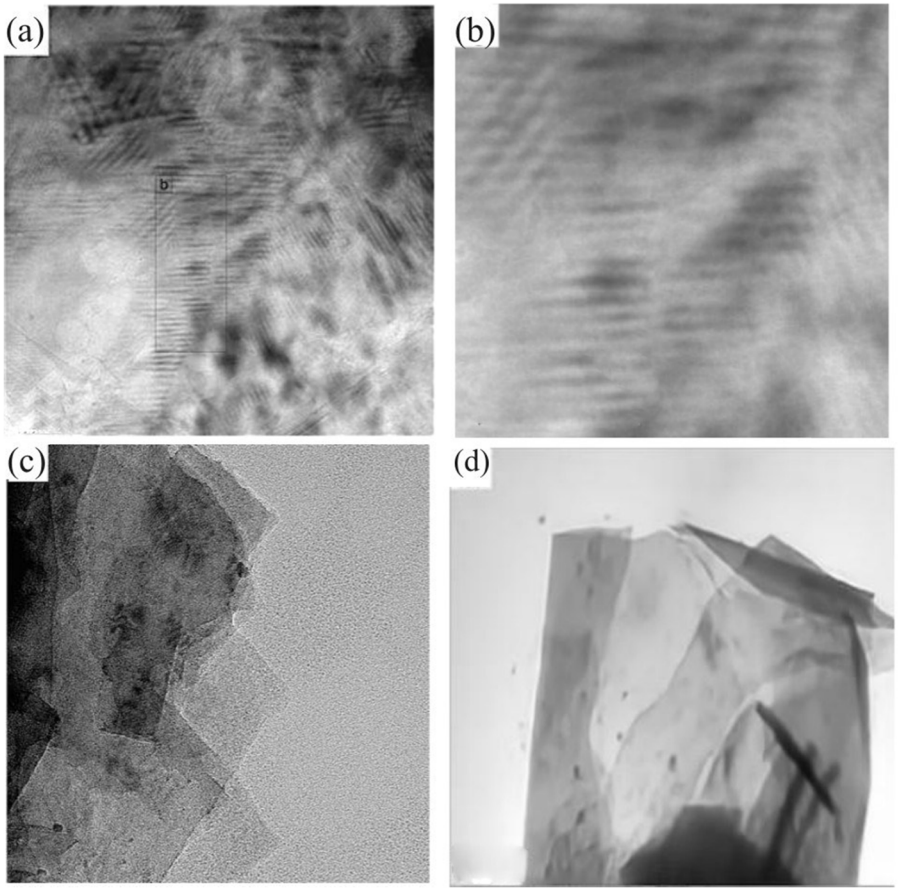


**Figure 5:** TEM photograph of GP40. (a) Longitudinal surface; (b) a partial enlarged view; (c) horizontal plane; (d) GP40 was ultrasonically dispersed in non-negative matrix factorization (NMF) and then dripped onto copper mesh for observation.

grinding, mixing, and dispersion (as shown in Figure 8), the continuous stripping of EG and graphene were realized, providing a new way for the preparation of graphene/polymer nanocomposites.

## 3.3 Structure and properties of graphene/elastomeric PVC nanocomposites

### 3.3.1 Structural morphology of graphene/elastomeric PVC nanocomposites

Figure 9 shows the SEM and TEM images of GE/CPE-PVC composites with 5% EG mass fraction. The SEM images show that the composite material maintains the morphology of the graphene fold lamellae at the macro level, and the graphene sheets are dispersed and embedded in the CPE-PVC matrix. TEM images of ultrathin slices of composite material show that the graphene sheets are evenly dispersed in the CPE PVC matrix, and the graphene sheets are bonded to each other to form conductive paths.

### 3.3.2 Electrical conductivity of graphene/elastomeric PVC nanocomposites

Here is the revised content with a more logical narrative sequence.

Figure 10 illustrates the relationship between the EG mass fraction and the volume conductivity of composite materials. Generally, the conductivity of the composite material increases with the EG content, demonstrating the formation of conductive networks as EG is incorporated. At a 3% EG mass fraction, the conductivity rises sharply by eight orders of magnitude, indicating the onset of conductive percolation where graphene sheets connect to form initial conductive pathways.

Between 3 and 4% EG mass fraction, the conductivity shows minimal variation, likely due to the stabilization of the network structure. However, when the EG mass fraction exceeds 4%, a second percolation phenomenon occurs, leading to another sharp increase in conductivity. At a 5% EG mass fraction, the composite exhibits good antistatic performance and achieves a conductivity of 0.22 S/m.

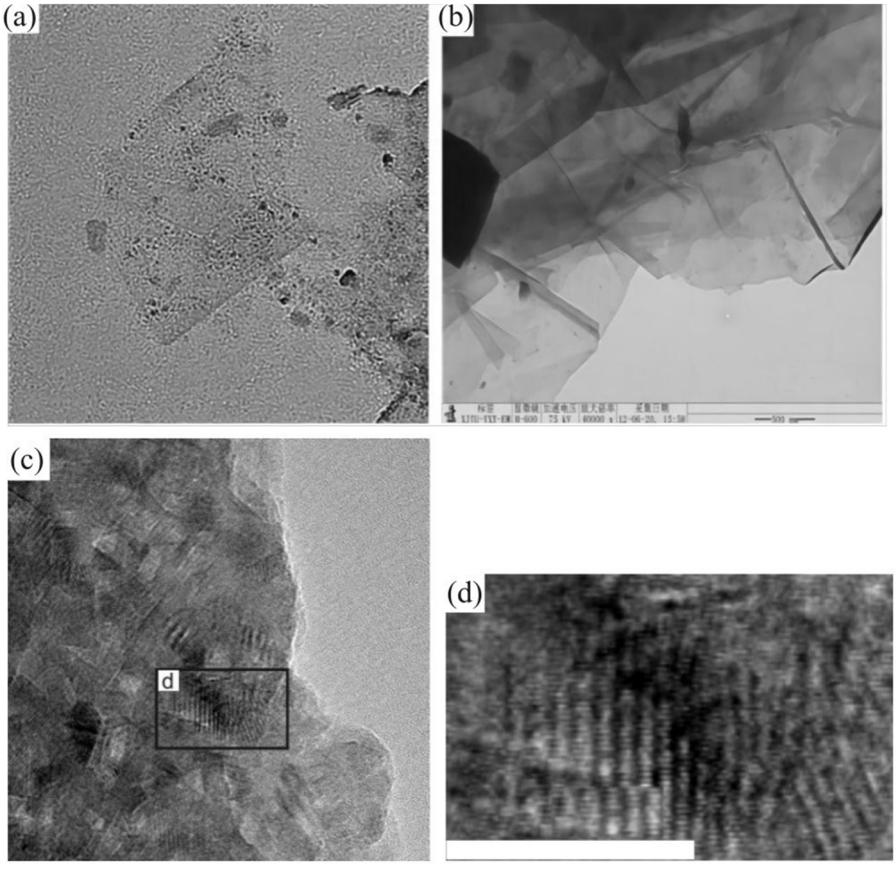


**Figure 6:** TEM image of graphene composite powder with 40% content (composite) powder. (a) Horizontal plane; (b) GCP40 was ultrasonically dispersed in NMF and then dropped onto copper mesh for observation; (c) longitudinal surfaces; (d) a partial enlarged view of (c).

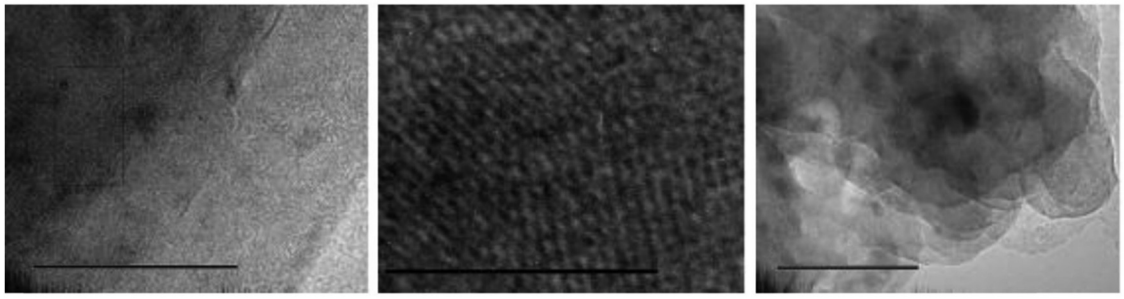

**Figure 7:** TEM image of EG-TPU-PVC composite powder.

Comparing different systems, the electrical conductivity of graphene/CPE-PVC composites is significantly enhanced compared to graphite/PVC nanocomposites. Furthermore, for the EG/TPU-PVC composite at a 5% EG mass fraction, the conductivity reaches 0.56 S/m. This improvement can be attributed to thinner graphite sheets, a higher degree of graphenization, and the formation of a more comprehensive conductive network as graphene sheets bond more effectively in the EG/PVC, EG/CPE-PVC, and EG/TPU-PVC systems, respectively.

### 3.3.3 Other properties of graphene/elastomeric PVC nanocomposites

Table 3 lists the electrical conductivity, thermal conductivity, electromagnetic shielding efficiency, and tensile strength of the graphene/elastomeric PVC composite.

Upon achieving a mass fraction of 5% in EG, the electrical conductivity, thermal conductivity and electromagnetic shielding efficiency of the nanocomposites from

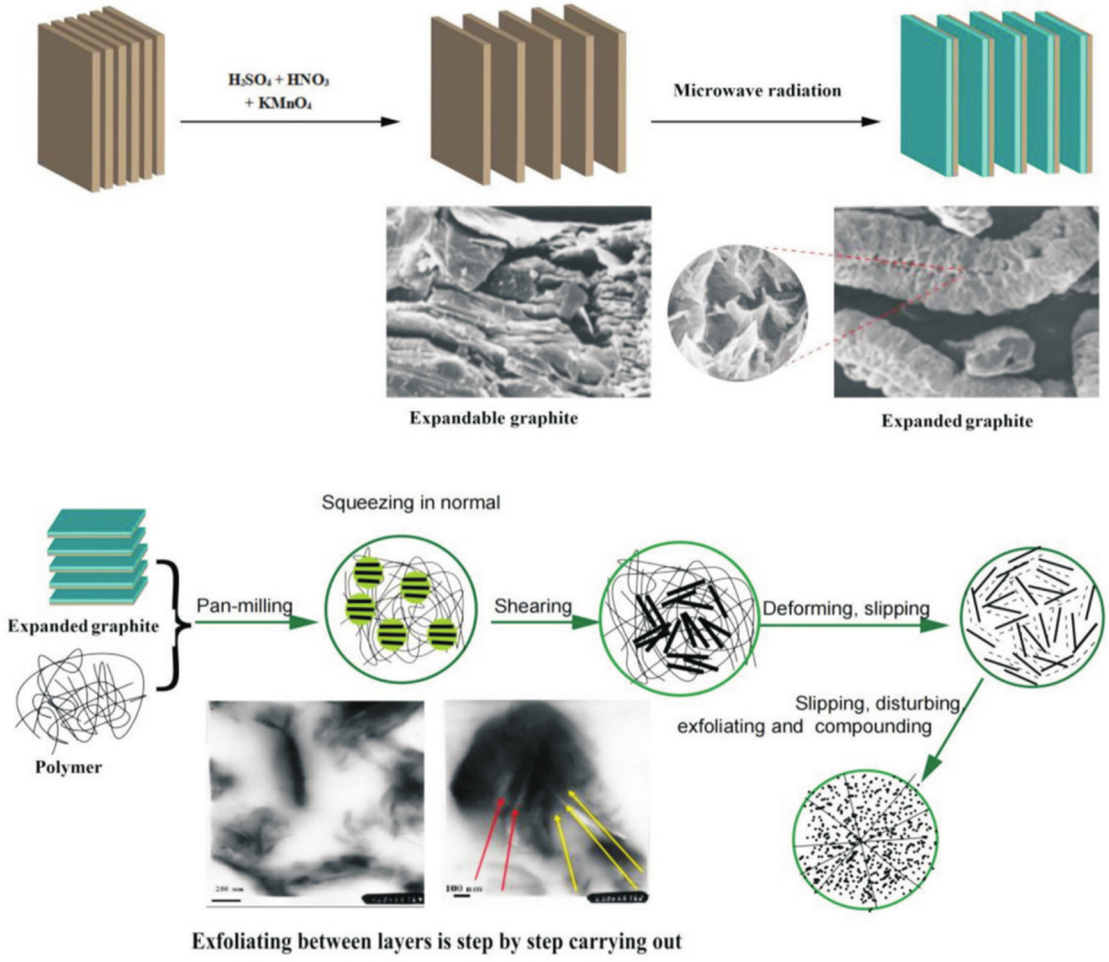


**Figure 8:** Graphitization process of graphite.

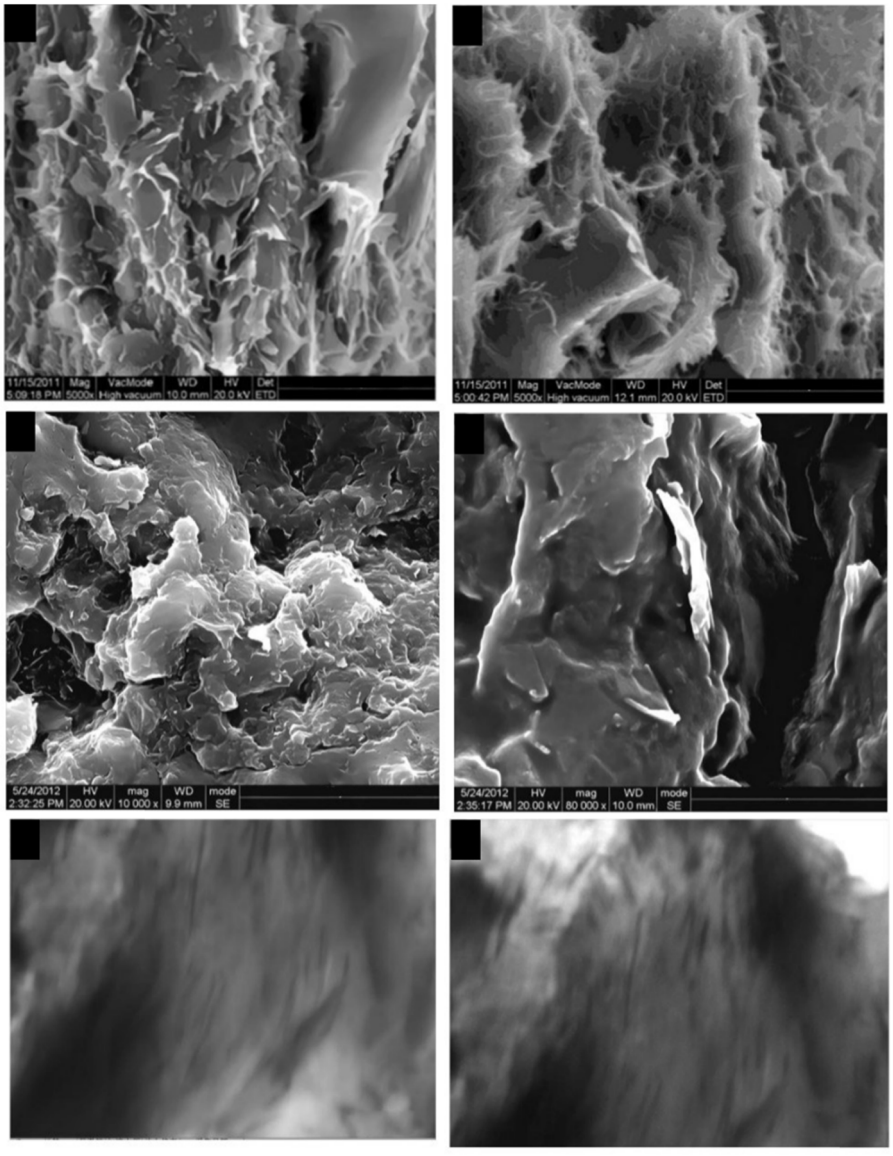

**Figure 9:** SEM and TEM images of graphene/PVC/CPE composites.

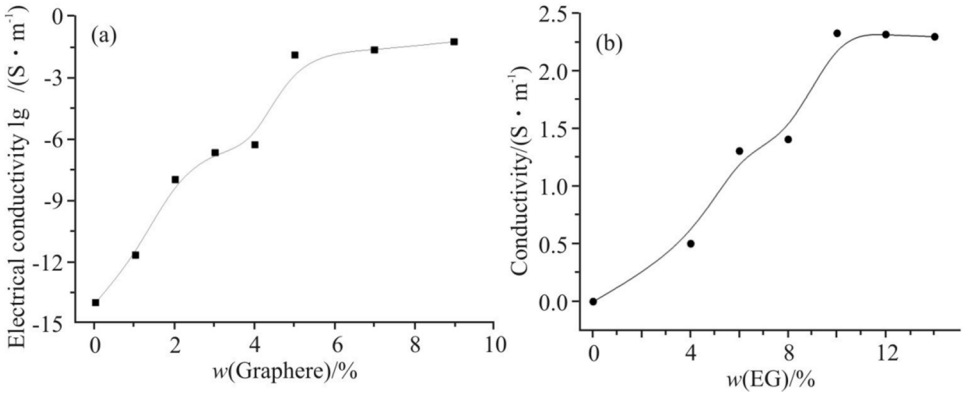


**Figure 10:** The effect of EG mass percentage on the graphene/elastomer PVC composites' conductivity. (a) Graphene/CPE-PVC composites; (b) graphene/TPU-PVC composites.

**Table 3:** Properties of graphene/elastomeric PVC composites

| Composite system (mass fraction, heat stabilizer 4%) | Electrical conductivity/(S $m^{-1}$) | Thermal conductivity/(W $m^{-1}$ $K^{-1}$) | EMSE$^{+}$/dB (thickness = 1.00 mm) | | Tensile strength/(MPa) |
|---|---|---|---|---|---|
| PVC | $10^{-15} \pm 10^{16}$ | 0.180 ± 0.006 | 3.00 ± 0.11 | 7.16 ± 0.23 | 20.34 ± 1.04 |
| EG/PVC (5/91) | $(4.2 \pm 0.14) \times 10^{-2}$ | 0.366 ± 0.013 | 23.73 ± 0.70 | 41.73 ± 1.26 | 27.94 ± 1.42 |
| EG/CPE-PVC (5/10/81) | 0.20 ± 0.02 | 0.464 ± 0.012 | 26.41 ± 0.77 | 44.88 ± 1.33 | 22.32 ± 1.10 |
| EG/TPU-PVC (5/10/81) | 0.57 ± 0.03 | 1.200 ± 0.034 | 28.00 ± 0.82 | 47.00 ± 1.43 | 25.30 ± 1.25 |

EG/PVC, EG/CPE-PVC to EG/TPU-PVC system increase successively. The results indicated that the graphene/elastomeric PVC nanocomposites were successfully prepared by the gradual graphenization of graphite in the grinding disk co-milling.

## 4 Conclusion

In this study, a novel multi-component polymer/graphite composite material was successfully prepared, with graphite effectively exfoliated and uniformly dispersed using the S3M method. By adjusting the combinations of PVC, CPE, and TPU, the distribution of graphite within the matrix was optimized, resulting in significantly improved conductivity and electromagnetic shielding efficiency. The results indicate that the electrical properties of the EG/PVC-CPE and EG/PVC-TPU systems are influenced by variations in the degree of graphite exfoliation and uniformity, which directly impact the electrical conductivity and electromagnetic shielding properties of the composites. In the EG/PVC-TPU system, the presence of single or even multiple layers of exfoliated graphite leads to higher electrical conductivity and excellent electromagnetic shielding performance. Additionally, the composite exhibits good mechanical strength and thermal stability, suggesting that this composite system holds great potential for practical applications, particularly in the development of EMI protection for electronic devices and high-conductivity materials.

The findings of this study offer new insights into the design and application of high-performance polymer/graphite composites. They further confirm the effectiveness of multi-component systems and the solid-state shear grinding method in optimizing composite properties, particularly in terms of electromagnetic shielding and electrical conductivity. Future research could explore additional filler and matrix combinations to further enhance the overall properties of composite materials and provide more reliable material solutions for advanced applications.

**Funding information:** Authors state no funding involved.

**Author contributions:** Conceptualization: Jiliang Xie and Li Chen; methodology: Yanxia Zeng; software: Jiliang Xie; validation: Jiliang Xie, Yanxia Zeng, and Xin Xiao; formal analysis: Xin Xiao; investigation: Xia Sun; resources: Li Chen; data curation: Xin Xiao; writing – original draft preparation: Jiliang Xie; writing – review and editing: Yanxia Zeng; visualization: Yanxia Zeng; supervision: Xin Xiao; project administration: Xia Sun; funding acquisition: Xia Sun. All authors have accepted responsibility for the entire content of this manuscript and approved its submission.

**Conflict of interest:** Authors state no conflict of interest.

**Data availability statement:** All data generated or analyzed during this study are included in this published article.

## References

[1] Cheng H, Zhang G, Liu X, Lin Y, Ma S, Lin G, et al. Achieving acceptable electromagnetic interference shielding in UHMWPE/ground tire rubber composites by building a segregated network of hybrid conductive carbon black. Nanocomposites. 2023;9(1):100–15.

[2] Zhang Y, Xu J, Zhang Z, Zhao L, Li M, Li M, et al. Mechanochemical synthesis of nanostructured and composite oxide ceramics: From mechanisms to tailored properties. Int J Appl Ceram Technol. 2024;21(2):616–54.

[3] Liao Y, Tan Q, Yang S, Chen Y, Chen G, Bai S. High value recycle of waste cross-linking polyethylene with the contribution of phosphogypsum to prepare composites. Waste Biomass Valoriz. 2023;14(11):3909–21.

[4] Zeng Y. A review of the research progress of composite bipolar plates for proton exchange membrane fuel cells with different substrate materials. Adv Eng Technol Res. 2023;8(1):517.

[5] Patti A, Acierno D. Structure-property relationships of waterborne polyurethane (WPU) in aqueous formulations. J Vinyl Addit Technol. 2023;29(4):589–606.

[6] Wang P, Liao Q, Zhang H. Polysaccharide-based double-network hydrogels: Polysaccharide effect, strengthening mechanisms, and applications. Biomacromolecules. 2023;24(12):5479–510.

[7] Elmi C. Physical-chemical properties of nano-sized phyllosilicates: recent environmental and industrial advancements. Encyclopedia. 2023;3(4):1439–60.
[8] Zhang Y, Wu H, Zhang W, Yang F. Polymer nanocomposites based on nano magnesium hydroxide. Chem Phys Polym Nanocompos: Process Morphol Struct Thermodyn Rheol. 2024;2:423–69.
[9] Yanga Y, Hua C, Liub Q, Lia J. Research progress and prospects of colored zirconia ceramics: A review. J Adv Ceram. 2024;13(10):1505–22.
[10] Boldyreva E. Spiers memorial lecture: Mechanochemistry, tribochemistry, mechanical alloying–retrospect, achievements and challenges. Faraday Discuss. 2023;241:9–62.
[11] Chen Y, Li J, Li T, Zhang L, Meng F. Recent advances in graphene-based films for electromagnetic interference shielding: Review and future prospects. Carbon. 2021;180:163–84.
[12] Verma S, Dhangar M, Mili M, Bajpai H, Dwivedi U, Kumari N, et al. Review on engineering designing of electromagnetic interference shielding materials using additive manufacturing. Polym Compos. 2022;43(7):4081–99.
[13] Liang X, Xu Y, Lin YE, Zhang C. Federated split learning via dynamic aggregation and homomorphic encryption on non-IID data. J Supercomput. 2025;81(1):63.
[14] Zahid M, Siddique S, Anum R, Shakir MF, Nawab Y, Rehan ZA. M-type barium hexaferrite-based nanocomposites for EMI shielding application: A review. J Supercond Nov Magn. 2022;34:1019–45.
[15] Gezahegn S, Garcia C, Lai R, Zhou X, Tjong J, Thomas SC, et al. Benign species-tuned biomass carbonization to nano-layered graphite for EMI filtering and greener energy storage functions. Renew Energy. 2021;164:1039–51.
[16] Sanghvi MR, Tambare OH, More AP. Performance of various fillers in adhesives applications: A review. Polym Bull. 2021;79(12):10491–553.
[17] Duan Y, Gao M, Pang H, Wang T. FeCoNiMnAl high-entropy alloy: Improving electromagnetic wave absorption properties. J Mater Res. 2022;36(10):2107–17.
[18] Jagadeeshanayaka N, Awasthi S, Jambagi SC, Srivastava C. Bioactive surface modifications through thermally sprayed hydroxyapatite composite coatings: A review of selective reinforcements. Biomater Sci. 2022;10(10):2484–523.
[19] Valencia L, Handa R, Monti S, Jasso-Salcedo AB, Georgouvelas D, Magaña I, et al. On the mineralization of nanocellulose to produce functional hybrid materials. J Mater Chem A. 2022;10(17):9248–76.